Modelling microplastic and solute dispersion in fluvial environments

Ben Stride[1], Soroush Abolfathi[1], Nipuni Odara Merenchi Galappaththige[1], Gary Bending[1], and Jonathon Pearson[1]

[1]University of Warwick

November 24, 2022

Abstract

Physical interactions of microplastics within vegetation and turbulent flows of freshwater systems are poorly understood. An experimental study was conducted to investigate the underlying physical transport mechanisms of microplastics over submerged canopies across a range of flow conditions common in the natural environment. The effects of changing canopy heights were investigated by testing two model canopies of varying stem heights, simulating seasonal variation. This study determined and compared the mixing and dispersion processes for microplastics and solutes and proposed a hydrodynamic model for quantifying microplastic mixing in submerged canopies. Longitudinal dispersion coefficients for neutrally buoyant microplastics (polyethylene) and solutes were significantly correlated within submerged model vegetation irrespective of the complexity of the flow regime. Hydrodynamic and solute transport models were shown to be capable of robust predictions of mixing for neutrally buoyant microplastics in environmental flows over a canopy, facilitating a new approach to quantify microplastic transport and fate.

Modelling microplastic and solute dispersion in fluvial environments

Dispersion of polyethylene in submerged model canopies

Ben Stride[a], Soroush Abolfathi[a], M.G.N. Odara[a], Gary D. Bending[b], Jonathan Pearson[a]

[a] School of Engineering, University of Warwick, Coventry CV4 7AL, UK

[b] School of Life Sciences, University of Warwick, Coventry CV4 7AL, UK

Highlights

- Neutrally buoyant microplastics (polyethylene) disperse in a similar manner to solutes (Rhodamine dye) within the water column of fluvial environments with submerged vegetation
- A novel fluorometric tracing and particle staining technique is proven to accurately trace stained microplastics within complex flow regimes in real-time
- A robust hydrodynamic model to predict mixing of neutrally buoyant microplastics is proposed
- Submerged vegetation creates distinct mixing zones over the depth, depending on the height of the canopy

Abstract

Physical interactions of microplastics within vegetation and turbulent flows of freshwater systems are poorly understood. An experimental study was conducted to investigate the underlying physical transport mechanisms of microplastics over submerged canopies across a range of flow conditions common in the natural environment. The effects of changing canopy heights were investigated by testing two model canopies of varying stem heights, simulating seasonal variation. This study determined and compared the mixing and dispersion processes for microplastics and solutes and proposed a hydrodynamic model for quantifying microplastic

mixing in submerged canopies. Longitudinal dispersion coefficients for neutrally buoyant microplastics (polyethylene) and solutes were significantly correlated within submerged model vegetation irrespective of the complexity of the flow regime. Hydrodynamic and solute transport models were shown to be capable of robust predictions of mixing for neutrally buoyant microplastics in environmental flows over a canopy, facilitating a new approach to quantify microplastic transport and fate.

Keywords

dispersion, canopy, microplastics, longitudinal dispersion, polyethylene, submerged vegetation

Teaser

We compare the mixing processes for microplastics and solutes then propose a hydrodynamic model for quantifying the mixing in submerged canopies.

1. Introduction

Over 5 trillion tonnes of plastic are afloat at sea (Eriksen et al., 2014) and up to 80% of plastics enter the ocean through river networks (Ockelford et al., 2020) causing potential long-term effects on ecosystems and ecosystem function. Detailed understanding of the underlying physical mechanisms that govern the behaviour, transport, and fate of plastics is needed to assess their impact on freshwater systems with complex flows (Abolfathi et al., 2020; Anderson et al., 2016; Bucci et al., 2020; Dris et al., 2018; Wagner et al., 2014). Plastic pollution is not only a concern because of the sheer volume being discarded, but because plastic polymers such as polyethylene (PE), polypropylene (PP), and polyvinyl chloride (PVC) are so resistant to degradation. These polymers can persist in the environment for centuries, enabling them to be transported far from their original source and often ending up in aquatic systems. Recent studies have shown plastics being found in the remotest of regions, including the six deepest ecosystems on earth (Jamieson et al., 2019) and sea ice in the Arctic (Peeken et al., 2018). When plastics do degrade, they break off in fragments from larger plastic objects and when smaller than 5 mm, plastic polymer fragments are defined as microplastics. There are many pathways microplastics can take to enter riverine ecosystems, from waste-water inputs to groundwater leaching, surface run-off, inappropriate waste management, and atmospheric deposition (Allen et al., 2019; Barnes et al., 2009; Horton et al., 2017; Klemeš et al., 2020; Talsness et al., 2009). PE and PP from tyres and road wear, along with abraded plastics from textiles during laundry, and broken-down packaging account for most of the plastic polymers transported by rivers in Europe (Horton et al., 2017; Rowley et al., 2020; Siegfried et al., 2017). Smaller sized plastics are considered a greater threat to humans and the environment (Edo et al., 2020) due to being easily ingested and significantly more abundant than large plastic particles (Erni-Cassola et al., 2017). Long-term effects of microplastic ingestion on human health are not fully understood but microplastics have recently been shown to accumulate in digestive tracts, blood streams, and lungs in humans (Jenner et al., 2022; Leslie et al., 2022; Miller et al., 2020; Sana et al., 2020).

Existing numerical models cannot robustly simulate the transport of microplastics in fluvial systems as there is limited physical modelling data to validate and calibrate such models. Solute transport models based upon the advection-diffusion equation have been meticulously developed (e.g. Elder, 1959; Fischer, 1966; Rutherford, 1994; Taylor, 1954) and are widely validated for tracer measurements across a wide range of flow domains including pipes, laboratory flumes, and natural rivers (e.g. Abolfathi & Pearson, 2017; Jimoh & Abolfathi, 2022). Thus, these models provide a suitable foundation to quantify the transport processes which govern pollution behaviour. Such models could also provide accurate approximations for the transport and dispersion of microplastics that have a similar density to solutes, where the assumption of a vertically well-mixed plume is valid. Most PE and PP particles have near neutral buoyancies of between 0.91-0.97 g/cm^3 and 0.9-0.91 g/cm^3, respectively (Emmerik & Schwarz, 2019), indicating that they may follow the same transport pathways as solutes in the natural environment. Cook et al. (2020a), proved that PE behaves analogous to solutes for open channel flow, suggesting solute transport models and fluorescent tracers can be used as a proxy for microplastics within “real-world” settings for this flow regime. Given that microplastics cannot be used for in situ tracer studies in freshwater systems, due to their hazardous impacts on the environment, it is important to understand how these particles can be mimicked by non-hazardous substances such as solute tracers (e.g. Rhodamine WT Dye).

Vegetation is ubiquitous in freshwater environments and alters the hydrodynamics of the system it is present within (Li & Zhang, 2010; Murphy et al., 2007; Shucksmith et al., 2011), making it a catalyst for altering the mixing processes of solutes. Within submerged vegetation, lower mean velocities are inside the vegetation canopy than that of the water column above (Lightbody & Nepf, 2006; Murphy et al., 2007; Nepf & Ghisalberti, 2008; Nepf et al., 1997) and flow paths become circuitous in motion as they bend around plant stems giving rise to variances in velocities (Nepf et al., 1997). These fluctuations in velocity generate distinct mixing regimes within the water column that vary over depth, and likely impact microplastic transport. Canopy height and density, along with river depth and discharge can vary depending on the season (Zhang et al., 2012) and climate change is expected to increase the frequency, intensity, and impacts of extreme weather events such as flooding and droughts (UK Centre for Ecology & Hydrology, 2021). With vegetation being more commonly used for flood protection (Geilen et al., 2004; Kourgialas & Karatzas, 2012; Vuik et al., 2016; Dong et al., 2020; Salauddin et al., 2021) and ever-present in fluvial systems, there is a significant need to quantify the impact of different canopy heights and densities on the transport and fate of microplastics. Recent research has documented the effects of microplastics on vegetation (De Souza Machado et al., 2019; Lehmann et al., 2020; Rillig et al., 2019) and the effects vegetation has on solute dispersion is well known (Li & Zhang, 2010; Lightbody & Nepf, 2006; Murphy et al., 2007; Nepf & Ghisalberti, 2008; Nepf et al., 1997; Shucksmith et al., 2011), but no research has been performed on the effects vegetation has on the dispersion of microplastics using solute transport techniques.

Fluorescent dyes such as Rhodamine WT dye have previously been used to trace concentrations of solutes within surface and groundwater studies (Chandler et al., 2016; Cook et al., 2020a and b; Harden at al., 2003; Nepf et al., 1997). If microplastics are shown to behave the same as fluorescent dyes under multiple flow regimes, then existing solute transport models can be applied to track and trace microplastics within different aquatic environments, ultimately determining their fate. Calculating the longitudinal dispersion coefficient (LDC) is one such method (Chikwendu, 1985; Elder, 1959; Taylor, 1954) and can be achieved through a variety of techniques such as fluorometry, Particle Image Velocimetry (PIV), and Planar Laser Induced Fluorescence (PLIF). Fluorometers can track fluorescent signatures, by detecting and quantifying them in real-time in both laboratory and field settings with relative ease. However, PIV and PLIF measurements require the use of lasers and shore-based cameras, causing them to be primarily implemented in laboratory-based studies over short timescales (Daigle et al., 2013).

Cook et al. (2020a) developed a method for chemically impregnating microplastics with Nile red dye (excitation/emission: 552/636 nm), which gives off a fluorescent signature similar to that of Rhodamine (excitation/emission: 555/580 nm), enabling them to be accurately traced in a laboratory or field setting using fluorometers in real-time in the same experimental setup (Fig.1). In the current study, this microplastic staining technique was adopted to trace PE's behaviour over submerged canopies with the aim of improving current understanding of the physical mechanisms that govern microplastic mixing and dispersion within these complex flows. The physical effects of vegetation were simulated in a laboratory flume using flexible straws, following previously proven methodological approaches (e.g. Li & Zhang, 2010; Murphy et al., 2007; Nepf & Ghisalberti, 2008; Nepf et al., 1997), and the effects of vegetation submergence depth on the transport behaviour of microplastics were quantified. Currently, there is limited data to validate the hypothesis of neutrally buoyant microplastics following similar transport pathways to that of solutes. LDC's for spherical neutrally buoyant PE were calculated and compared with those measured from Rhodamine WT dye and analytical solutions for the advection-diffusion equation were adopted to propose a mixing model for neutrally buoyant microplastics of a similar density to water. This paper, for the first time, identified and quantified the underlying mixing mechanisms of microplastics for complex flows over a submerged canopy.

2. Material and Methods

2.1 Experimental setup

Spherical PE (434272, Sigma-Aldrich) of 40-46 µm in diameter was used due to it being one of the most common plastic polymers found in rivers across the globe (Emmerik and Schwarz, 2019; Horton et al. 2017; Rowley et al., 2020). Spherical PE particles represent a class of microplastics which are neutrally buoyant and therefore can be modelled using solute transport techniques. The PE was stained with Nile red dye (technical grade, N3013, Sigma-Aldrich) and Rhodamine WT dye was employed as the fluorescent solute to be used as a comparison for the dispersion of PE. Longitudinal dispersion measurements were conducted in a 0.34 m wide, 20 m long recirculating rectangular flume (Fig. 1) made from glass reinforced plastic with a depth ranging from 0.248-0.254 m due to the variability at higher flow rates and differing vegetation conditions. The wave dissipating weir was 4.5 m long (depending on angle) and acted as a downstream tailgate that could be altered to maintain the flow depth of 0.25 m. Velocities for the concentration data were calculated relative the position of the top fluorometers through Eq. (1) and highlighted in Fig. 1 as F1, F2, F3, and F4.

$$u = \frac{F_4 - F_1}{\mu_4 - \mu_1}, \tag{1}$$

where F_4 and F_1 represent the location of the fourth and first fluorometers within the flume and μ_4 and μ_1 is the travel time between the centroids (s) of the fourth and first fluorometers respectively. The top fluorometers were selected for the main LDC results due to the excitation and emission of light covering a larger proportion of the water column, especially within the mixing and free flow zones (see §2.5). Bottom fluorometers were used for supplementary data and labelled F5, F6, F7, and F8. Velocity data for the *N*-zone model was collected using an

Acoustic Doppler Velocimeter (ADV) positioned near the centre of the flow length section to accurately record 3D water velocity measurements.

Concentration data was gathered through fluorometers positioned 2.6 m apart at 20º angles, ensuring maximum detection of the tracer cloud in the centre of the flow and encompassing its distribution at depth. The fluorometers used Rhodamine WT optics with a linear range of 0-1000 ppb and a minimum detection limit of 0.01 ppb so that both Rhodamine dye and Nile red stained PE could be traced. To test the quality of data measurements recorded by the fluorometers, linear calibrations were performed in which an R^2 value > 0.99 was obtained and used to convert voltages to ppb and mg/l for both dye and PE. Fluorometers used a x10 gain, logged at a rate of 10 Hz, and are illustrated by grey rectangles emitting a green light in the experimental setup (Fig. 1). Plastic straws were glued into circular divots made in the simulated channel bed (made of PVC sheets) designed to imitate a uniform dense vegetation canopy and removed for the base condition of open-channel flow. These are highlighted in green in Fig. 1 and Fig. 2.

2.2 Experimental Processes

Three experimental scenarios were designed for this study including one scenario with ‘no vegetation’ (NV), and two scenarios with a canopy of varying stem heights. Vegetation lengths of 0.1 m for low vegetation (LV), and 0.2 m for high vegetation (HV) were chosen (Fig. 2) and removed for the base condition of open-channel flow. The LV and HV flow regimes contained $\frac{H}{h_1}$ values of 2.5 and 1.25 in that order, where H is the channel depth (m) and h_1 is the height of the vegetation canopy. Each straw had a diameter of 4 mm and was placed in equally spaced rectangles 25 mm from the straw in front of it (parallel to the flow direction) and 50 mm from the straw to beside it. Subsequently, a fifth straw was inserted in the middle of each rectangle. Three replicates were used for both Rhodamine and PE injections for four different depth-averaged velocities of 0.0588 m/s, 0.1059 m/s, 0.1529 m/s, and 0.2 m/s in accordance with both Cook et al. (2020a) and Guymer (2002) to approximate velocities experienced by UK rivers. These were logged for 6, 5, 4, and 3 minutes respectively within each of the different canopy heights. Logging started and stopped at least 30 seconds before and after fluorescence was injected/detected. Injections were made before the flow inlet from the pump which was located before the first straws within the flume (Fig. 1). 10 ml of Rhodamine WT at 3000 ppb and 1.5 g of Nile red stained PE with < 10 ml of water was well-mixed into a syringe before each injection. Table 1 provides a summary of these different conditions. Reynolds numbers for each velocity were calculated through Eq. (2):

$$Re = \frac{uH}{v}, \tag{2}$$

where u is the velocity (m/s) and v is the kinematic viscosity (m²/s).

Velocity data can only be retrieved at least 40 mm away from the end of the ADV transmitter, requiring predictions to be made for the top 40-50 mm of the water column. Correlations and velocities were averaged from all four beams produced by the ADV to ensure quality data. If velocity measurements had correlation values below 0.8, they were highlighted and removed. Spikes in the ADV data were highlighted using a threshold calculated from the surrounding datapoints and replaced using a smoothed estimate outlined in Goring & Nikora (2002). Sampling for velocity measurements occurred at a rate of 100 Hz for a 5-minute duration for each 32 mm range over the 250 mm water depth in the flume for each flow condition. For the vegetative conditions, fitted velocity measurements were interpolated using a polynomial function in order to produce uniformly distributed velocity profiles over the water column. Open channel flow velocities were theoretically predicted using logarithmic law through rearranging Eq. (3):

$$u_* = \frac{uk}{LN\left(\frac{H}{y0}\right)} \tag{3}$$

u_* represents shear velocity from the bottom of the channel (m/s), k is the Von Karman constant, H is the mean channel depth (m), and $y0$ is the relative roughness of the channel bed (depending on the material) divided by 30 for hydraulically rough flows. Examples of these profiles can be seen below for the differing flow rates of 5 l/s (0.0588 m/s), 9 l/s (0.1059 m/s), 13 l/s (0.1529 m/s), and 17 l/s (0.2m/s) in Fig. 3.

2.3 longitudinal dispersion

Taylor's (1954) fundamental analysis is widely recognized as a proven technique for calculating the longitudinal dispersion of a solute within turbulent flow. Taylor (1954) found that after an adequate amount of time, a solute being injected into a cross-sectional area containing a solvent exhibiting uniform flow conditions will form a Gaussian distribution along the longitudinal axis as seen in Fig. 4. Using a Fickian diffusion-type expression within the one-dimensional advection-diffusion equation (ADE) this effect is shown in Eq. (4)

$$\frac{\partial c}{\partial t} + u\frac{\partial c}{\partial t} = D_x \frac{\partial^2 c}{\partial x^2}, \qquad (4)$$

D_x is the longitudinal dispersion coefficient in m²/s and considers the effects of advection, molecular diffusion, and shear dispersion, c represents the cross-sectional mean concentration (kg/m³), t is time (s), x is distance (m). LDC's were generated from the temporal concentration distribution of each tracer injection. Background removal was implemented by subtracting the mean of the last 25 seconds of data collection for each concentration curve. Cutoff values for the start and end of the peaks were selected using approximately 5% of the peak concentration and were checked by plotting the values on the respective distributions. Smoothing was implemented through a running average containing 1 % of the total number of data points, enabling a larger or smaller window to be implemented depending on the logging length/flow rate. Moments of the distributions were calculated and a regression was fitted to calculate the gradient of time to centroid against the variance. LDC's were then established through Eq. (5) and confidence intervals of LDC's were determined by first calculating the standard deviation (σ_x^2) and applying an α value of 5%.

$$D_x = \frac{1}{2}u^2\frac{d\sigma_x^2}{dt}. \qquad (5)$$

2.4 Modelling longitudinal dispersion

Given an idealized vertical velocity profile, Elder (1958) created an equation that can theoretically predict D_x by accounting for the effects of shear dispersion through Eq. (6)

$$D_x = 5.93 H u_*, \tag{6}$$

Rutherford (1994) showed that u_* can be calculated through simply dividing the depth-averaged velocity u by anywhere between 10 and 20 depending on the roughness of the riverbed. This method was used as a reference for calculating u_* and applying logarithmic law in open channels through Eq. (3). Elder's (1958) equation is widely used due to its simplicity and that it is based on fundamental mechanisms that are widely accepted. However, Elder's (1958) equation assumes a logarithmic velocity profile across the depth of the channel and does not account for potential fluctuations in velocity. Chikwendu (1986) developed an *N*-zone model that can be divided into an infinite number of zones (j) in agreement with Taylor's (1954) original formulas. Mixing in each zone is dependent on the velocity differences of the zones either side of it $\left(q_1 + q_2 + \cdots + q_j\right)^2\left[1 - \left(q_1 + q_2 + \cdots + q_j\right)\right]^2\left[u_{1,2\ldots j} - u_{(j+1)\ldots N}\right]^2$ divided by the vertical diffusivity $b_{j(j+1)}$ with the longitudinal diffusivity $\sum_{j=1}^{N} q_j D_{xj}$ added to the total

$$D_x(N) = \sum_{j=1}^{N-1} \frac{\left(q_1+q_2+\cdots+q_j\right)^2\left[1-\left(q_1+q_2+\cdots+q_j\right)\right]^2\left[u_{1,2\ldots j}-u_{(j+1)\ldots N}\right]^2}{b_{j(j+1)}} + \sum_{j=1}^{N} q_j D_{xj}, \tag{7}$$

$j = (1,2, \ldots N)$, $q = \frac{h_j}{H}$, D_{xj} is the average longitudinal diffusivity, and h_j is the thickness of each zone. The average vertical diffusivity between each zone is calculated by

$$b_{j(j+1)} = \frac{2 D_{zj(j+1)}}{H^2\left(q_j + q_{j+1}\right)}, \tag{8}$$

where $D_{zj(j+1)} = H k u_* q(1-q)$ using Elder's (1958) equation for vertical diffusivity or $\frac{k u_* H}{6}$ when using a depth-averaged value (Jobson and Sayre, 1970).

2.5 *Modelling longitudinal dispersion in vegetated flows*

Vegetation makes the hydrology within river systems more complex and harder to model and/or predict the transport and fate of the pollutant in question. Reynolds stress and velocities vary over depth (Fig. 5) therefore a logarithmic velocity profile cannot be assumed when submerged vegetation is present. Longitudinal dispersion is consequently split into zones of mixing that vary over the vertical in size and number depending on the vegetation conditions present. These can include a wake zone, a mixing zone, and a free flow zone which is illustrated in Fig. 5. Using Chikwendu's (1986) model Shucksmith et al. (2011) calculated $D_{zj(j+1)}$ by considering both the velocity and shear stress profiles to represent the vertical diffusivity within the system more accurately in Eq. (9). Vertical shear stress can be approximated through Reynolds stress in the mixing zone, assuming a Schmidt number of 1, defined as the net transfer of momentum across a surface within a turbulent fluid because of fluctuations in velocity.

$$D_{zj(j+1)} = \frac{\tau_j}{\rho \frac{du}{dz_j}}, \tag{9}$$

ρ is the density of the fluid and τ_j is the Reynolds stress in each zone j (N/m²). Within the wake zone a uniform velocity will occur because of low velocity gradients causing $\frac{du}{dz}$ to be near zero and Eq. (9) to become redundant as limited mixing will take place due to shear. Mixing within the wake zone is expected to be mainly through diffusivity and Lightbody and Nepf's (2006) emergent salt marsh canopy equation can be used to calculate $D_x(N)$

$$D_x(N) = 0.17uS_d, \tag{10}$$

where u is the depth-averaged velocity in the wake zone. Above dense vegetation canopies the velocity profile can become logarithmic again in the free flow zone and the top of the canopy acts as another boundary layer requiring a need to estimate an equivalent shear velocity (Murphy et al. 2007; Shucksmith et al., 2011).

$$u_{*hc} = \sqrt{gh_2S_0}, \tag{11}$$

where g is acceleration due to gravity (m²/s), h_2 is the height of free flow zone, and S_0 represents the bed slope. Therefore, using u_{*hc} mean vertical diffusivity $D_{zj(j+1)}$ in the free flow zone can be calculated as

$$\frac{Hku_{*hc}}{6}. \quad (12)$$

3. Results

3.1 *Concentration Data*

LDC's are displayed on the right-hand side of Table 1 and range from 0.0031 ± 0.0006 to 0.0140 ± 0.0016 m²/s for both dye and PE within open channel flow for velocities ranging from 0.0588 – 0.2000 m/s. LDC's sorted by canopy height and including confidence intervals can be seen in Table S1, supplementary material. A few LDC's for the vegetative conditions overlapped on Fig. 6 but generally dispersion increased with canopy height (h_1) compared to overall depth (0.25 m) and velocity. LV ($\frac{H}{h_1}$ = 2.5) LDC's ranged from 0.0115 ± 0.0039 to 0.0487 ± 0.0042 m²/s and HV ($\frac{H}{h_1}$ = 1.25) LDC's ranged from 0.0166 ± 0.0017 to 0.0707 ± 0.0060 m²/s, both in line with Shucksmith et al's. (2011) cropped vegetation and Murphy et al's. (2007) model canopy values. R^2 values > 0.95 for LDC's against velocity were achieved for every condition (Fig. 6). Using equation (1) velocities for both dye and PE were comparative to each other across all flow regimes ranging from 0.05827 ± 0.0002 m/s for the flow rate of 5 l/s to 0.209215 ± 0.0005 m/s for 20 l/s.

3.2 *N-zone Model*

LDC's for both dye and PE were compared to Chikwendu's (1986) *N*-zone model across all test conditions. For NV the *N*-zone model achieved a factor ($\frac{D_x}{Hu_*}$) of 5.93 in line with Elder's (1958) equation when using both an idealised velocity profile from the channel bed and a $\frac{u}{u_*}$ of 19.3. Resultingly, the *N*-zone model provided analogous results to the mean LDC's for both dye and PE shown in Fig. 6. The $\frac{D_x}{Hu_*}$ values for LV and HV of 15.6 and 34.3 reinforce existing theory suggesting submerged vegetation velocity profiles differ from a logarithmic boundary layer due to the creation of a semipermeable boundary layer generated through drag created at the top of the canopy (Ghisalberti & Nepf, 2005). Using Shucksmith's (2011) adaptation of Chikwendu's (1986) *N*-zone model, accurate LDC's were predicted for the LV and HV conditions. LDC's appeared to show more variability for the HV condition (Fig. 6) and at higher velocities, which is expected due to increased turbulence and resultingly higher noise level produced by fluorometers being positioned closer to the canopy. Rhodamine dye and PE demonstrated analogous relationships with the *N*-zone model through root mean square values (RMSE) and percent differences (Table 2). Overall, *N*-zone predicted LDC's were within 10 % for every experimental condition, specifically within 9.32 % accuracy for dye, and 9.83 % accuracy for PE under the NV, LV, and HV regimes (Table 2).

3.3 Microplastics versus dye

The LDC regressions and both the percentage difference and RMSE analysis indicate that PE dispersed equally to dye across all flow regimes. The largest percentage differences happened between PE and dye and the *N*-zone model within the slowest depth-averaged velocities of 0.0588 m/s (5 l/s) and 0.1059 m/s (9 l/s) across all the conditions. This was potentially due to the dispersion coefficients being low themselves, exaggerating the differences (Table S1) or minor differences between PE and dye dispersion due to PE being slightly less than neutrally buoyant and advection playing a less dominant role at lower velocities. Further analysis between the raw LDC data for dye and PE within the slowest depth-averaged velocities revealed no significant difference between the two populations (Welch's *t*-test $p > 0.05$). For six of the eight flow rates within the vegetated conditions (Table S1), dye and PE percent differences were dispersing within a 15.06 % range of each other and within 6.12 % for each vegetated condition (Table 2). This was supported through the regression containing an R^2 value of 0.98 and a gradient of 1.06x when dye and PE were plotted against each other (Fig. 7). The RMSE analysis displayed slightly better values using dye as the predicted value for PE dispersion than the *N*-zone model, indicating that dye is an agreeable substitute when used as a proxy for neutrally buoyant microplastic movement. As expected, LDC's and variability (95 % confidence intervals) increased with higher velocities as shown by the regression and longer error bars in Fig. 7.

4. Discussion

4.1 Applicability of microplastic tracing and hydrodynamic modelling

Fluorometers calibrated for Rhodamine emission and excitation wavelengths of 555 nm and 580 nm were found to accurately predict neutrally buoyant microplastic dispersion in complex flow regimes, widening their current proven applicability from open channels to additional flow environments. In theory, fluorometric techniques can be utilised to trace stained solid particles of a near neutral buoyancy displaying the correct wavelengths for the employed instruments. Crucially, this demonstrates ample opportunity within future research to calculate the dispersion of any pollutant that meets these criteria. As a result, the applicability of fluorometric tracing can be significantly widened beyond solutes. Since PE is a solid particle and not a solute, the response curves generate more scattered dispersion bands, causing the voltage readings to vary slightly as the particles pass through the optical sensor. This does not affect the calculated dispersion, as demonstrated in Cook et al. (2020a) and we would expect the same phenomenon to occur for other stained solid particles used for fluorometric tracing. Although dye produced marginally improved results when modelling PE dispersion, the N-zone model predicted LDC's to within 5.72 % across the vegetated conditions (Table 2), thus analysing velocities over depth may be used to reasonably predict the dispersion of spherical neutrally buoyant PE in fluvial environments. It is then a logical assumption that other hydrodynamic models that use velocity profiles may also provide insights into microplastic dispersion and may be used to quantify their mixing given the right conditions.

4.2 Flow characteristics

The flow physics for both the LV and HV conditions are visualized in Fig. 2 and modelled in Fig. 5. The LV profiles are dominated by vortex driven exchanges that penetrate deep into the canopy where they reach the riverbed and are shot back out into the free flow zone. This causes the entire canopy to become a singular mixing zone, thus eliminating the wake zone (Fig. 5). The LV condition displayed flow characteristics similar to Shucksmith et al's (2011) Carex plants at a height of 0.055 m, despite Shucksmith implementing a changing overall depth relative to the canopy height and ours being constant at 0.25 m, due to vortices penetrating to the bed in both cases. The LV condition was also analogous to Murphy et al's (2007) sparse canopy setting indicating that within these flow environments, vortices dominate the mixing processes. Thus, vortices govern longitudinal dispersion in submerged vegetation if they penetrate to the bed, producing two zones of mixing. At the lowest depth-averaged velocity of 0.0588 m/s, the velocity profile for LV in Fig. 3 exhibits a noticeable linear trend over depth when compared to other velocities for this condition. Indicating that below a certain velocity, the differences between the mixing and free flow region are not significant enough to cause the canopy to exhibit a constant velocity at any stage over depth compared to a slight drag displayed in the top half of the canopies for the faster depth-averaged velocities of 0.1059 m/s, 0.1529 m/s, and 0.2 m/s. The HV profiles are split into three separate zones where vortices from the free flow zone dominate the dispersion and only reach so far into the vegetation canopy, enabling separate mixing and wake zones to be established (Fig. 5). The HV condition matched Shucksmith's (2011) other cropped cases where the mixing was split into three zones instead of two. Dispersion occurs mostly in the mixing and free flow zones with very little contributing within the canopy wake zone. Identification of mixing zone penetration depth to the top of the wake zone (z_1) when using the *N*-zone model is therefore essential to accurately depict the flow physics of the channel. Reynolds stress profiles from the ADV were used over the depth to predict the size of each zone and determine whether a wake zone was indeed present.

Reynolds stress for the vegetative conditions differed due to its impact on both the velocity and concentration profiles. Reynolds stress peaked at the top of the canopy (h_1) and at the bed of the flume, indicating two boundary layers are present within vegetative flow (shown in Fig. 5) in accordance with Murphy et al. (2007) and Shucksmith et al. (2011). Reynolds stress values for each condition were predicted using an approximation of turbulent eddies via Eq. (9). As flow rates increased, the Reynolds stress also increased causing more extreme profiles over the depth at the top of the canopy. Reynolds stress values within the wake zone were often negative, once again producing the need to provide an accurate representation of the mixing zone penetration depth within the *N*-zone model and correctly implement Eq. (10), eliminating these negative values. Highlighting how many zones are present within the system is consequently instrumental to performing the correct analysis within the *N*-zone model. With this in mind, mixing zone penetration depth can also be achieved through Eq. (13):

$$\frac{z_2}{h_1} = \frac{CSL}{C_d N_v S_d h_1}, \tag{13}$$

where CSL is the canopy shear layer parameter with an empirical value of 0.23 ± 0.06 (Nepf et al., 2007), C_d is the vegetation drag coefficient, N_v is the vegetation density, and S_d is the stem diameter. Although this is a good reference for mixing zone penetration depth, Shucksmith et al. (2011) demonstrated it can be more accurately interpreted from Reynolds stress.

With the flow inlet from the pump in Fig. 1 being perpendicular to the direction of the flow a honeycomb structure was implemented to straighten the flow (Fig. 1) after a visible bifurcation effect originally caused $\frac{D_x}{Hu_*}$ to be lower for the base condition of open channel flow. Bifurcation is particularly rare within real-world settings and therefore not applicable to this study, however within open channel flow the initial tests resulted in the flow physics producing a low $\frac{D_x}{Hu_*}$ when measured against the concentration data. Based on these results, bifurcation causes lower LDC's when employing fluorometric techniques. This is potentially due to the bulk of both the dye and PE concentrations snaking around certain fluorometers instead of flowing through the optical sensors. More research is needed on the effect bifurcation has on longitudinal dispersion inside open channels, but it is outside the scope of this study. For future studies, when using flumes that have pipes perpendicular to the channel (Fig. 1), implementing a honeycomb structure to straighten the flow is recommended.

4.3 Solute and microplastic dispersion

LDC's for neutrally buoyant microplastics (i.e. PE) and solutes (i.e. Rhodamine dye) were significantly correlated within submerged model vegetation irrespective of the complexity of the flow regime (i.e. Reynolds number) in the water column. The complexity of the flow regime within the water column did not affect microplastic dispersion inversely to a conventional solute such as Rhodamine. It is therefore reasonable to expect that microplastics of a near neutral buoyancy behave in the same manner as solutes from the riverbed to the flow surface no matter how fast or complicated the flow regime may be. The findings highlight that microplastics similar to those tested in this study will eventually be deposited in the ocean and not retained within river catchments once they enter the water column of fluvial systems. It is worth noting we observed a visible "wall creeping" effect for a small percentage of the microplastics as seen in Eitzen et al. (2019) study. PE particles would attach themselves to the model vegetation or the glass walls of the flume through adsorption, but this was not a significant amount when compared to the bulk tracer cloud that advected straight through. Nizzetto et al's. (2016) study inferred that microplastics with a diameter of < 0.2 mm were not retained in river catchments regardless of their density and only 16-38 % of microplastics with a higher density than water were retained. Below a certain size other factors such as shape and density become less significant because the smaller the particle, the lower the effect of the gravitational force and the higher the effect of the surface force that can act on them. Hoellein et al. (2019) suggested that particle shapes can affect microplastic transport, but also stated that even after biofilm colonization, if the density of the microplastic was less than water it would float. Drummond et al. (2022) also approximated only 5 % of microplastics were subject to long-term accumulation per km in rivers, all supporting our findings that the majority of neutrally buoyant microplastics follow the same transport pathways as solutes and are not retained in river catchments. Over long timescales however, this small percentage is subject to incremental change and will likely become significant given large enough quantities resulting in microplastics potentially accumulating in “dead zones” within rivers (Guymer, 2002; Wallis et al., 1989). Though, when subjected to turbulent flows these adsorbed microplastics may saltate over longer durations (Ji et al., 2014) resulting in temporary reintroductions into the main flow within the water column and once again reaching the ocean given a long enough timescale.

We recognize that the results of this data are limited to spherical PE particles but ultimately contribute to the end goal of validating solute transport techniques to accurately predict neutrally buoyant microplastic dispersion. It is expected that biofouling, along with different microplastic types, sizes, shapes, and densities may affect the transport and fate of microplastics above a certain size (Besseling et al., 2017; Bucci et al., 2020; Hoellein et al., 2019; Kaiser et al., 2017, Nizzetto et al., 2016). If particles are below this size, we would expect similar results for other plastic polymers regardless of their type or shape if they have a near neutral buoyancy such as PP. Density and size may then be the most important factors for smaller microplastics but, as suggested by Nizzetto et al. (2016), even microplastics with higher densities may not be retained in rivers if they are below a certain diameter. This study, for the first time, proposes and validates a dispersion model suitable for neutrally buoyant microplastics within complex flows influenced by submerged canopies. These results can consequently contribute to implementing a new technique for identifying the transport and fate of microplastics within rivers worldwide. To provide a more comprehensive understanding of the underlying mechanisms affecting microplastic transport these variables (e.g. particle’s type, size, shape, and density) need to be investigated over a variety of timescales and flow conditions to identify and quantify these effects on the dispersion of microplastics.

5. Conclusion

The dispersion and mixing processes of PE microplastics over submerged canopies were investigated using novel fluorometric tracing and particle staining techniques for the first time within a laboratory setting. The fluorometric and hydrodynamic analysis showed that distinct mixing zones were created over the canopy, which were primarily influenced by canopy characteristics (i.e. stem height). Neutrally buoyant PE dispersed interchangeably with Rhodamine in the water column regardless of the complexity of the flow regime instigated by submerged model vegetation. The results of the fluorometric analysis showed that Rhodamine WT dye can be used as a proxy over short timescales for field tests with spherical microplastics of a near neutral buoyancy (i.e. PE) in free-surface flows containing vegetated environments. It was shown that analytical solutions for mixing coefficients, as a result of the advection-diffusion equation and hydrodynamic modelling using velocity profiles (the *N*-zone model), are capable of accurately approximating PE mixing and dispersion over a canopy for a range of environmental flows with varying Reynolds numbers. Consequently, the proposed analytical solutions and newly developed tracing and staining techniques for determining the transport and fate of neutrally buoyant microplastics can help develop effective management strategies to enhance water quality across a variety of turbulent flow domains in the future.

6. Acknowledgements

6.1 Funding

Funding was provided by the Natural Environmental Research Council (NERC) and The Central England NERC Training Alliance (CENTA). We also acknowledge our Civil Engineering Technician Ian Bayliss for help in setting up the experiment.

NERC grant NE/S007350/1 (243303, BS)

7. Declarations

7.1 Author Contributions

Conceptualization: BS, JP, MGNO
Investigation: BS, JP, SA
Methodology: BS, JP, MGNO
Supervision: JP, SA, GB
Visualization: BS, SA
Writing-original draft: BS

Writing-review and editing: BS, JP, SA, GB

7.2 Competing Interests

We confirm that none of the material has been published or is under consideration for publication elsewhere, and we have no conflicts of interest to declare.

7.3 Data and materials availability

All data used in the analysis, including MATLAB code can be made available in the supplementary materials.

References

Abolfathi, S., Cook, S., Yeganeh-Bakhtiary, A., Borzooei, S., & Pearson, J. (2020). Microplastics Transport and Mixing Mechanisms in the Nearshore Region. *Coastal Engineering Proceedings*, *36v*, 63. https://doi.org/10.9753/icce.v36v.papers.63

Abolfathi, S., & Pearson, J. (2017). Application of Smoothed Particle Hydrodynamics (Sph) in Nearshore Mixing: a Comparison To Laboratory Data. *Coastal Engineering Proceedings*, *35*, 16. https://doi.org/10.9753/icce.v35.currents.16

Allen, S., Allen, D., Phoenix, V. R., Le Roux, G., Jimenez, P. D., Simonneau, A., Binet, S., Galop, D. (2019). Atmospheric transport and deposition of microplastics in a remote mountain catchment. *Nature Geoscience, 12*, 339–344. https://doi.org/10.1038/s41561-019-0335-5

Barnes, D. K. A., Galgani, F., Thompson, R. C., & Barlaz, M. (2009). Accumulation and fragmentation of plastic debris in global environments. *Philosophical Transactions of the Royal Society B: Biological Sciences*, *364*(1526), 1985–1998. https://doi.org/10.1098/rstb.2008.0205

Besseling, E., Quik, J. T. K., Sun, M., & Koelmans, A. A. (2017). Fate of nano- and microplastic in freshwater systems: A modeling study. *Environmental Pollution*, *220*, 540–548. https://doi.org/10.1016/j.envpol.2016.10.001

Bucci, K., Tulio, M., & Rochman, C. M. (2020). What is known and unknown about the effects of plastic pollution: A meta-analysis and systematic review. *Ecological Applications*, *30*(2), 1–16. https://doi.org/10.1002/eap.2044

Chandler, I. D., Guymer, I., Pearson, J. M., & van Egmond, R. (2016). Vertical variation of mixing within porous sediment beds below turbulent flows. *Water Resources Research*, *52*, 3493–3509. https://doi.org/10.1111/j.1752-1688.1969.tb04897.x

Chikwendu, S. C. (1986). Application of a slow-zone model to contaminant dispersion in laminar shear flows. *International Journal of Engineering Science*, *24*(6), 1031–1044. https://doi.org/10.1016/0020-7225(86)90034-0

Cook, S., Chan, H. L., Abolfathi, S., Bending, G. D., Schäfer, H., & Pearson, J. M. (2020a). Longitudinal dispersion of microplastics in aquatic flows using fluorometric techniques. *Water Research*, *170*, 115337. https://doi.org/10.1016/j.watres.2019.115337

Cook, S., Price, O., King, A., Finnegan, C., van Egmond, R., Schäfer, H., Pearson, J. M., Abolfathi, S., & Bending, G. D. (2020b). Bedform characteristics and biofilm community development interact to modify hyporheic exchange. *Science of the Total Environment*, *749*, 141397. https://doi.org/10.1016/j.scitotenv.2020.141397

Daigle, A., Bérubé, F., Bergeron, N., & Matte, P. (2013). A methodology based on Particle image velocimetry for river ice velocity measurement. *Cold Regions Science and Technology*, *89*, 36–47. https://doi.org/10.1016/j.coldregions.2013.01.006

de Souza Machado, A. A., Lau, C. W., Kloas, W., Bergmann, J., Bachelier, J. B., Faltin, E., Becker, R., Görlich, A. S., & Rillig, M. C. (2019). Microplastics Can Change Soil Properties and Affect Plant Performance. *Environmental Science and Technology*, *53*(10), 6044–6052. https://doi.org/10.1021/acs.est.9b01339

Dong, S., Abolfathi, S., Salauddin, M., Tan, Z. H., & Pearson, J. M. (2020). Enhancing climate resilience of vertical seawall with retrofitting - A physical modelling study. *Applied Ocean Research*, *103*(February), 102331. https://doi.org/10.1016/j.apor.2020.102331

Dris, R., Imhof, H. K., Löder, M. G. J., Gasperi, J., Laforsch, C., & Tassin, B. (2018). Microplastic contamination in freshwater systems: Methodological challenges, occurrence and sources. In Microplastic Contamination in Aquatic Environments: An Emerging Matter of Environmental Urgency. https://doi.org/10.1016/B978-0-12-813747-5.00003-5

Drummond, J. D., Schneidewind, U., Li, A., Hoellein, T. J., Krause, S., & Packman, A. I. (2022). Microplastic accumulation in riverbed sediment via hyporheic exchange from headwaters to mainstems. *Science Advances*, *8*(2). https://doi.org/10.1126/sciadv.abi9305

Edo, C., González-Pleiter, M., Leganés, F., Fernández-Piñas, F., & Rosal, R. (2020). Fate of microplastics in wastewater treatment plants and their environmental dispersion with effluent and sludge. *Environmental Pollution*, *259*. https://doi.org/10.1016/j.envpol.2019.113837

Eitzen, L., Paul, S., Braun, U., Altmann, K., Jekel, M., & Ruhl, A. S. (2019). The challenge in preparing particle suspensions for aquatic microplastic research. *Environmental Research*, *168*, 490–495. https://doi.org/10.1016/j.envres.2018.09.008

Elder, J. W. (1958). The dispersion of marked fluid in turbulent shear flow. *Journal of Fluid Mechanics*, *5*(4), 544–560. https://doi.org/10.1163/9789004326910

Eriksen, M., Lebreton, L. C. M., Carson, H. S., Thiel, M., Moore, C. J., Borerro, J. C., Galgani, F., Ryan, P. G., & Reisser, J. (2014). Plastic Pollution in the World's Oceans: More than 5 Trillion Plastic Pieces Weighing over 250,000 Tons Afloat at Sea. *PLoS ONE*, *9*(12), 1–15. https://doi.org/10.1371/journal.pone.0111913

Erni-cassola, G., Gibson, M. I., Thompson, R. C., & Christie-oleza, J. A. (2017). Lost, but Found with Nile Red: A Novel Method for Detecting and Quantifying Small Microplastics (1 mm to 20 μ m) in Environmental Samples. *Environmental Science & Technology*, *51*, 13641–13648. https://doi.org/10.1021/acs.est.7b04512

Fischer, H. (1966). Longitudinal Dispersion in Laboratory and Natural Streams. *Technical Report.* Keck Laboratory of Hydraulic and Water Resources, California Institution of Technology, Pasadena, California.

Geilen, N., Jochems, H., Krebs, L., Muller, S., Pedroli, B., van der Sluis, T., van Looy, K., & van Rooij, S. (2004). Integration of ecological aspects in flood protection strategies: Defining an ecological minimum. *River Research and Applications, 20*(3), 269–283. https://doi.org/10.1002/rra.777

Goring, D. G., & Nikora, V. I. (2002). Despiking Acoustic Doppler Velocimeter Data. Journal of Hydraulic Engineering, 128(1), 117–126. https://doi.org/10.1061/(asce)0733-9429(2002)128:1(117)

Guymer, I., & Environment Agency. (2002). *A national database of travel time, dispersion and methodologies for the protection of river abstractions.*

Harden, H. S., Chanton, J. P., Rose, J. B., John, D. E., & Hooks, M. E. (2003). Comparison of sulfur hexafluoride, fluorescein and rhodamine dyes and the bacteriophage PRD-1 in tracing subsurface flow. *Journal of Hydrology*, *277*, 100–115. https://doi.org/10.1016/S0022-1694(03)00074-X

Hoellein, T. J., Shogren, A. J., Tank, J. L., Risteca, P., & Kelly, J. J. (2019). Microplastic deposition velocity in streams follows patterns for naturally occurring allochthonous particles. *Scientific Reports*, *9*(1), 1–11. https://doi.org/10.1038/s41598-019-40126-3

Horton, A. A., Svendsen, C., Williams, R. J., Spurgeon, D. J., & Lahive, E. (2017). Large microplastic particles in sediments of tributaries of the River Thames, UK – Abundance, sources and methods for effective quantification. *Marine Pollution Bulletin*, *114*(1), 218–226. https://doi.org/10.1016/j.marpolbul.2016.09.004

Jamieson, A. J., Brooks, L. S. R., Reid, W. D. K., Piertney, S. B., Narayanaswamy, B. E., & Linley, T. D. (2019). Microplastics and synthetic particles ingested by deep-sea amphipods in six of the deepest marine ecosystems on Earth. *Royal Society Open Science*, *6*(2), 1–11. https://doi.org/10.1098/rsos.180667

Ji, C., Munjiza, A., Avital, E., Xu, D., & Williams, J. (2014). Saltation of particles in turbulent channel flow. *Physical Review E - Statistical, Nonlinear, and Soft Matter Physics*, *89*(5), 1–14. https://doi.org/10.1103/PhysRevE.89.052202

Jimoh, M., & Abolfathi, S. (2022). Modelling pollution transport dynamics and mixing in square manhole overflows. *Journal of Water Process Engineering*, *45*(August 2021), 102491. https://doi.org/10.1016/j.jwpe.2021.102491

Jenner, L. C., Rotchell, J. M., Bennett, R. T., & Cowen, M. (2022). Science of the Total Environment Detection of microplastics in human lung tissue using μ FTIR spectroscopy. *Science of the Total Environment*, *831*(March), 154907. https://doi.org/10.1016/j.scitotenv.2022.154907

Jobson, H.E., & Sayre, W.W. (1970). Vertical Transfer in Open Channel Flow. *Journal of Hydraulic Engineering*, *96*, 703-724.

Kaiser, D., Kowalski, N., & Waniek, J. J. (2017). Effects of biofouling on the sinking behavior of microplastics. *Environmental Research Letters*, *12*(12). https://doi.org/10.1088/1748-9326/aa8e8b

Khatmullina, L., & Isachenko, I. (2017). Settling velocity of microplastic particles of regular shapes. *Marine Pollution Bulletin*, *114*(2), 871–880. https://doi.org/10.1016/j.marpolbul.2016.11.024

Klemeš, J. J., Fan, Y. Van, Tan, R. R., & Jiang, P. (2020). Minimising the present and future plastic waste, energy and environmental footprints related to COVID-19. *Renewable and Sustainable Energy Reviews*, *127*(April). https://doi.org/10.1016/j.rser.2020.109883

Kourgialas, N. N., & Karatzas, G. P. (2013). A hydro-economic modelling framework for flood damage estimation and the role of riparian vegetation. *Hydrological Processes, 27*(4), 515–531. https://doi.org/10.1002/hyp.9256

Lehmann, A., Leifheit, E. F., Feng, L., Bergmann, J., Wulf, A., & Rillig, M. C. (2020). Microplastic fiber and drought effects on plants and soil are only slightly modified by arbuscular mycorrhizal fungi. *Soil Ecology Letters*. https://doi.org/10.1007/s42832-020-0060-4

Leslie, H. A., J. M. van Velzen, M., Brandsma, S. H., Vethaak, D., Garcia-Vallejo, J. J., & Lamoree, M. H. (2022). Discovery and quantification of plastic particle pollution in human blood. *Environment International*, 107199. https://doi.org/10.1016/j.envint.2022.107199

Li, C. W., & Zhang, M. L. (2010). 3D modelling of hydrodynamics and mixing in a vegetation field under waves. *Computers and Fluids*, *39*(4), 604–614. https://doi.org/10.1016/j.compfluid.2009.10.010

Li, J., Liu, H., & Paul Chen, J. (2018). Microplastics in freshwater systems: A review on occurrence, environmental effects, and methods for microplastics detection. *Water Research*, *137*, 362–374. https://doi.org/10.1016/j.watres.2017.12.056

Lightbody, A. F., & Nepf, H. M. (2006). Prediction of velocity profiles and longitudinal dispersion in emergent salt marsh vegetation. *Limnology and Oceanography*, *51*(1), 218–228. https://doi.org/10.4319/lo.2006.51.1.0218

Miller, M. E., Hamann, M., & Kroon, F. J. (2020). Bioaccumulation and biomagnification of microplastics in marine organisms: A review and meta-analysis of current data. *PLoS ONE*, *15*, 1–25. https://doi.org/10.1371/journal.pone.0240792

Murphy, E., Ghisalberti, M., & Nepf, H. (2007). Model and laboratory study of dispersion in flows with submerged vegetation. *Water Resources Research*, *43*(5), 1–12. https://doi.org/10.1029/2006WR005229

Nepf, H. M., & Ghisalberti, M. (2008). Flow and transport in channels with submerged vegetation. *Acta Geophysica*, *56*(3), 753–777. https://doi.org/10.2478/s11600-008-0017-y

Nepf, H. M, Ghisalberti, M., White, B., & Murphy, E. (2007). Retention time and dispersion associated with submerged aquatic canopies. Water Resources Research, 43(4), 1–10. https://doi.org/10.1029/2006WR005362

Nepf, H. M., Mugnier, C. G., & Zavistoski, R. A. (1997). The effects of vegetation on longitudinal dispersion. *Estuarine, Coastal and Shelf Science*, *44*(6), 675–684. https://doi.org/10.1006/ecss.1996.0169

Nizzetto, L., Bussi, G., Futter, M. N., Butterfield, D., & Whitehead, P. G. (2016). A theoretical assessment of microplastic transport in river catchments and their retention by soils and river sediments. *Environmental Science: Processes and Impacts*, *18*(8), 1050–1059. https://doi.org/10.1039/c6em00206d

Ockelford, A., Cundy, A., & Ebdon, J. E. (2020). Storm Response of Fluvial Sedimentary Microplastics. *Scientific Reports*, *10*, 1–10. https://doi.org/10.1038/s41598-020-58765-2

Peeken, I., Primpke, S., Beyer, B., Gütermann, J., Katlein, C., Krumpen, T., Bergmann, M., Hehemann, L., & Gerdts, G. (2018). Arctic sea ice is an important temporal sink and means of transport for microplastic. *Nature Communications*, *9*(1), 1–12. https://doi.org/10.1038/s41467-018-03825-5

Rillig M. C., Lehmann, A., de Souza Machado, A. A., Yang, G. (2019). Microplastic Effects on Plants. *New Phytologist*, *223,* 1066–1070. https://doi.org/10.1111/nph.15794

Rowley, K. H., Cucknell, A. C., Smith, B. D., Clark, P. F., & Morritt, D. (2020). London's river of plastic: High levels of microplastics in the Thames water column. *Science of the Total Environment, 740.* https://doi.org/10.1016/j.scitotenv.2020.140018

Rutherford, J.C. (1994). River Mixing. *John Wiley and Sons*, New York

Sana, S. S., Dogiparthi, L. K., Gangadhar, L., Chakravorty, A., & Abhishek, N. (2020). Effects of microplastics and nanoplastics on marine environment and human health. *Environmental Science and Pollution Research*, *27*(36), 44743–44756. https://doi.org/10.1007/s11356-020-10573-x

Salauddin, M., O'Sullivan, J. J., Abolfathi, S., & Pearson, J. M. (2021). Eco-Engineering of Seawalls—An Opportunity for Enhanced Climate Resilience From Increased Topographic Complexity. *Frontiers in Marine Science*, *8*(June), 1–17. https://doi.org/10.3389/fmars.2021.674630

Siegfried, M., Koelmans, A. A., Besseling, E., & Kroeze, C. (2017). Export of microplastics from land to sea. A modelling approach. *Water Research*, *127*, 249–257. https://doi.org/10.1016/j.watres.2017.10.011

Shucksmith, J. D., Boxall, J. B., & Guymer, I. (2011). Determining longitudinal dispersion coefficients for submerged vegetated flow. *Water Resources Research*, *47*(10), 1–13. https://doi.org/10.1029/2011WR010547

Talsness, C. E., Andrade, A. J. M., Kuriyama, S. N., Taylor, J. A., & Saal, F. S. V. (2009). Components of plastic: Experimental studies in animals and relevance for human health. *Philosophical Transactions of the Royal Society B: Biological Sciences, 364*(1526), 2079–2096. https://doi.org/10.1098/rstb.2008.0281

Taylor, G. (1954). The dispersion of matter in turbulent flow through a pipe. *Proceedings of the Royal Society of London. Series A. Mathematical and Physical Sciences*, *223*(1155), 446–468. https://doi.org/10.1098/rspa.1954.0130

UK Centre for Ecology and Hydrology. Retrieved 8th of November 2021 from https://www.ceh.ac.uk/future-flows-river-flow-changes-season

van Emmerik, T., & Schwarz, A. (2020). Plastic debris in rivers. *Wiley Interdisciplinary Reviews: Water, 7*(1), 1–24. https://doi.org/10.1002/wat2.1398

Vuik, V., Jonkman, S. N., Borsje, B. W., & Suzuki, T. (2016). Nature-based flood protection: The efficiency of vegetated foreshores for reducing wave loads on coastal dikes. *Coastal Engineering, 116*, 42–56. https://doi.org/10.1016/j.coastaleng.2016.06.001

Wagner, M., Christian, S., Diana, A.-M., Nicole, B., Xavier, B., Sebastian, B., Elke, F., Cecile, G., Jorg, K., Teresa, M., Sara, R.-M., Ralph, U., Dick, V., Margrethe, W.-N., & Georg, R. (2014). Microplastics in freshwater ecosystems: what we know and what we need to know. *Environmental Sciences Europe*, *26*, 1–12. https://doi.org/10.1186/s12302-014-0012-7

Wallis, S. G., & Beven, K. J. (1989). Transport in Stream Channels. *Proceedings of the Institution of Civil Engineers*, *87(1)*(May), 1–22

Zhang, W., Mu, S. S., Zhang, Y. J., & Chen, K. M. (2012). Seasonal and interannual variations of flow discharge from Pearl River into sea. *Water Science and Engineering,* *5*(4), 399–409. https://doi.org/10.3882/j.issn.1674-2370.2012.04.004

Tables

Table 1. *Summary of experimental flow conditions and parameters. Where n is the number of replicates, u_* is the bed shear velocity and u_{*hc} is the shear velocity at the top of the vegetation canopy*

											Longitudinal Dispersion Coefficient (m^2/s)		
n	Flow Rate (l/s)	Average Velocity (m/s)	Average Canopy Velocity (m/s)	Average Free Flow Velocity (m/s)	Flow Depth (m)	Canopy Height (m)	Stem Diameter (m)	Reynolds Number	u_*	u_{*hc}	Measured Dye	Measured PE	*N*-zone
3	5	0.060	N/A	N/A	0.25	0	0.004	14245	0.0031	N/A	0.0037	0.0031	0.0046
3	5	0.047	0.022	0.064	0.25	0.1	0.004	11124	0.0024	0.0384	0.0148	0.0112	0.0094
3	5	0.053	0.040	0.093	0.25	0.2	0.004	12686	0.0027	0.0221	0.0191	0.0166	0.0226
3	9	0.108	N/A	N/A	0.25	0	0.004	25777	0.0056	N/A	0.0075	0.0085	0.0083
3	9	0.083	0.037	0.114	0.25	0.1	0.004	19675	0.0043	0.0384	0.0222	0.0156	0.0202
3	9	0.102	0.077	0.183	0.25	0.2	0.004	24130	0.0052	0.0221	0.0327	0.0329	0.0449
3	13	0.155	N/A	N/A	0.25	0	0.004	36858	0.0079	N/A	0.0118	0.0110	0.0119
3	13	0.120	0.063	0.158	0.25	0.1	0.004	28585	0.0062	0.0384	0.0312	0.0341	0.0288
3	13	0.136	0.107	0.229	0.25	0.2	0.004	32159	0.0070	0.0221	0.0503	0.0451	0.0510
3	17	0.208	N/A	N/A	0.25	0	0.004	49524	0.0107	N/A	0.0139	0.0140	0.0159
3	17	0.154	0.079	0.204	0.25	0.1	0.004	36580	0.0079	0.0384	0.0466	0.0487	0.0498
3	17	0.159	0.127	0.263	0.25	0.2	0.004	37579	0.0081	0.0221	0.0655	0.0707	0.0570

Table 2. *LDC root mean square error (RMSE) comparison between dye, PE, and the N-zone model for the different vegetated conditions*

				RMSE		
Vegetation Condition	% Difference PE vs Dye	% Difference Dye vs *N*-zone	% Difference PE vs *N*-zone	PE vs Dye	Dye vs *N*-zone	PE vs *N*-zone
NV	0.56	9.32	9.83	0.00069	0.00117	0.00130
LV	4.49	6.12	1.36	0.00417	0.00350	0.00366
HV	1.42	5.56	5.76	0.00391	0.00763	0.01006

Figures

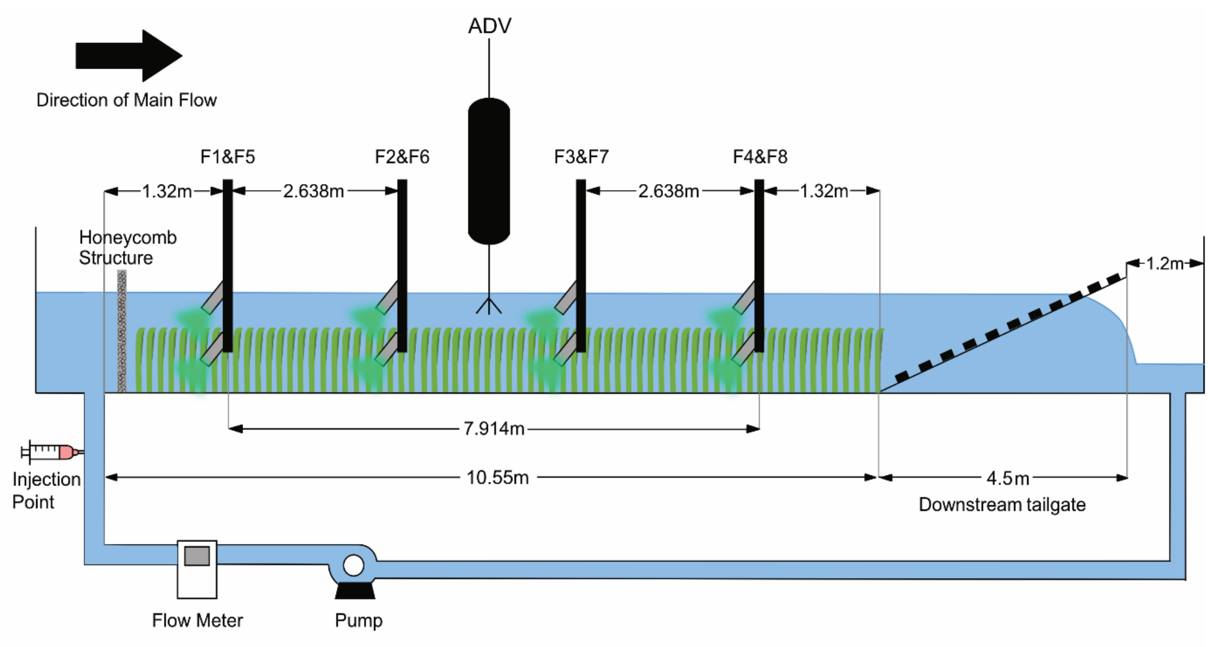

Fig. 1. *2D Illustration of the experimental flume set-up (not to scale)*

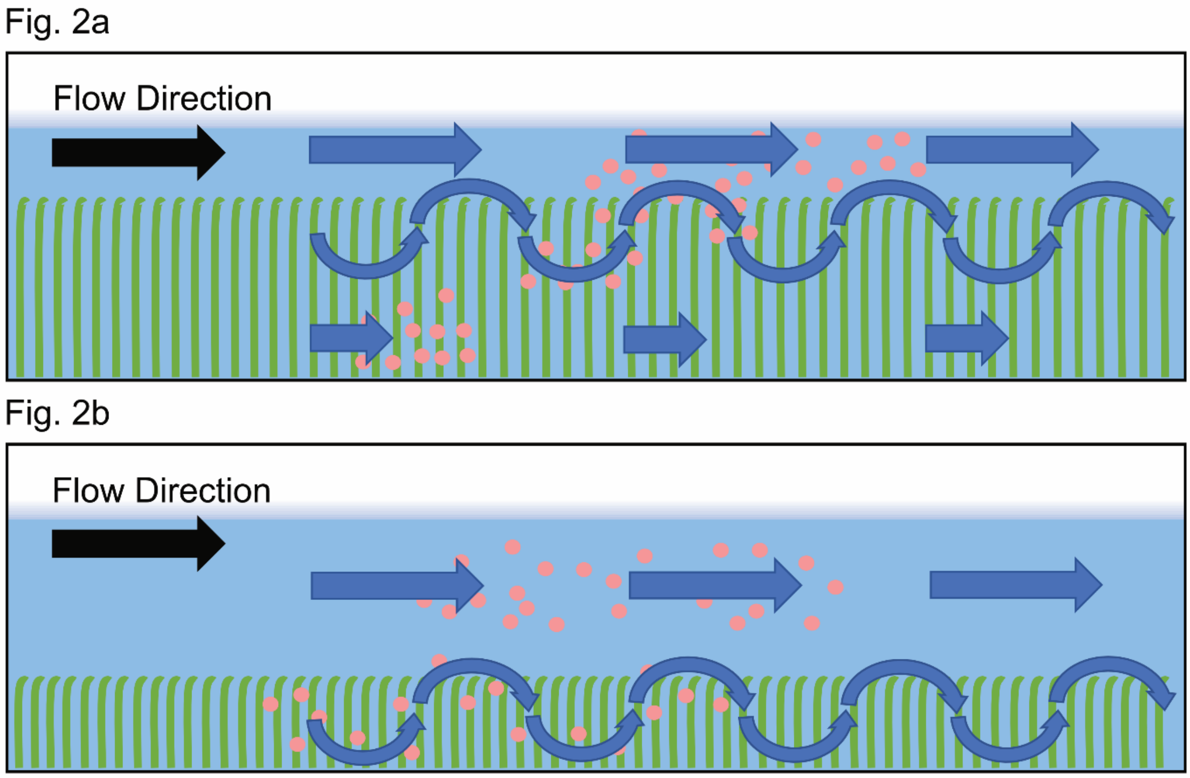

Fig. 2. *Visual illustration of the flow physics within Fig. 2a high (0.2 m) and Fig. 2b low (0.1 m) canopy heights in relation to a constant depth (0.25 m)*

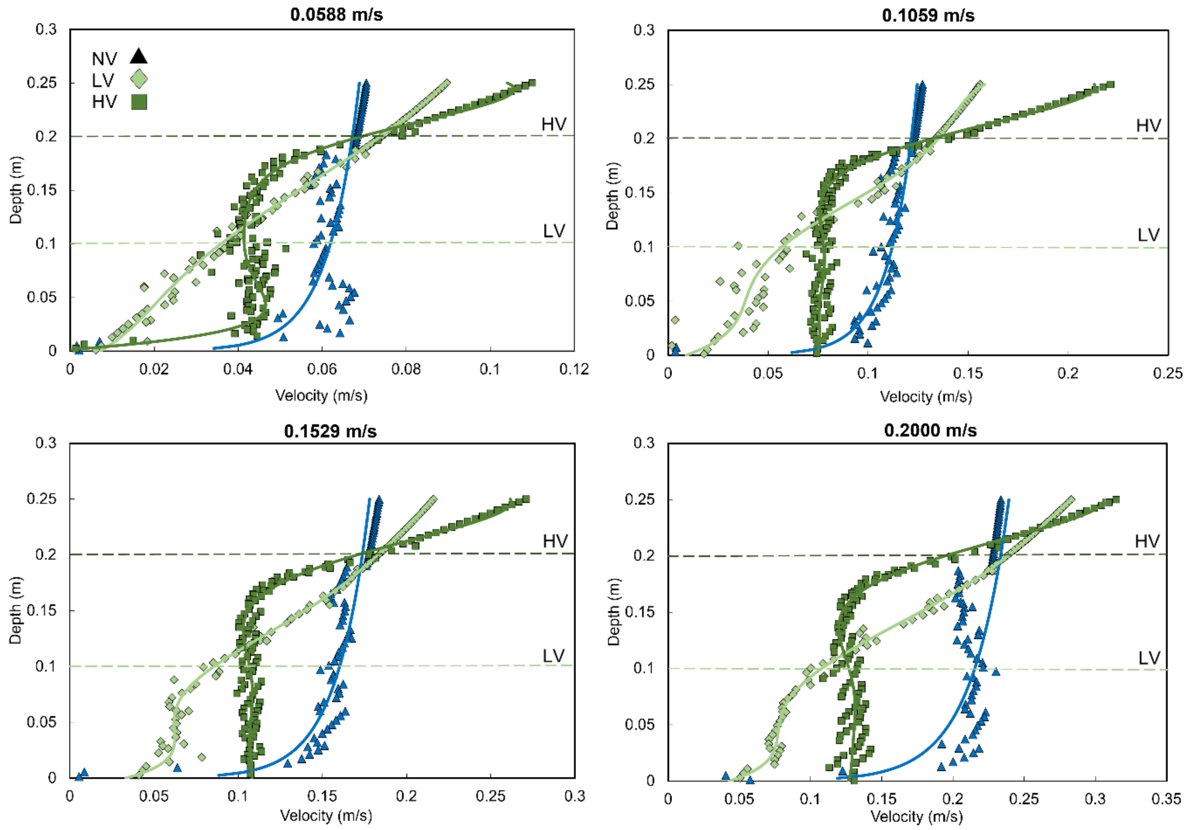

Fig. 3. *Fitted and measured velocity profiles for 0.0588, 0.1059, 0.1529, 0.2000 m/s depth-averaged velocities within the NV, LV, and HV conditions*

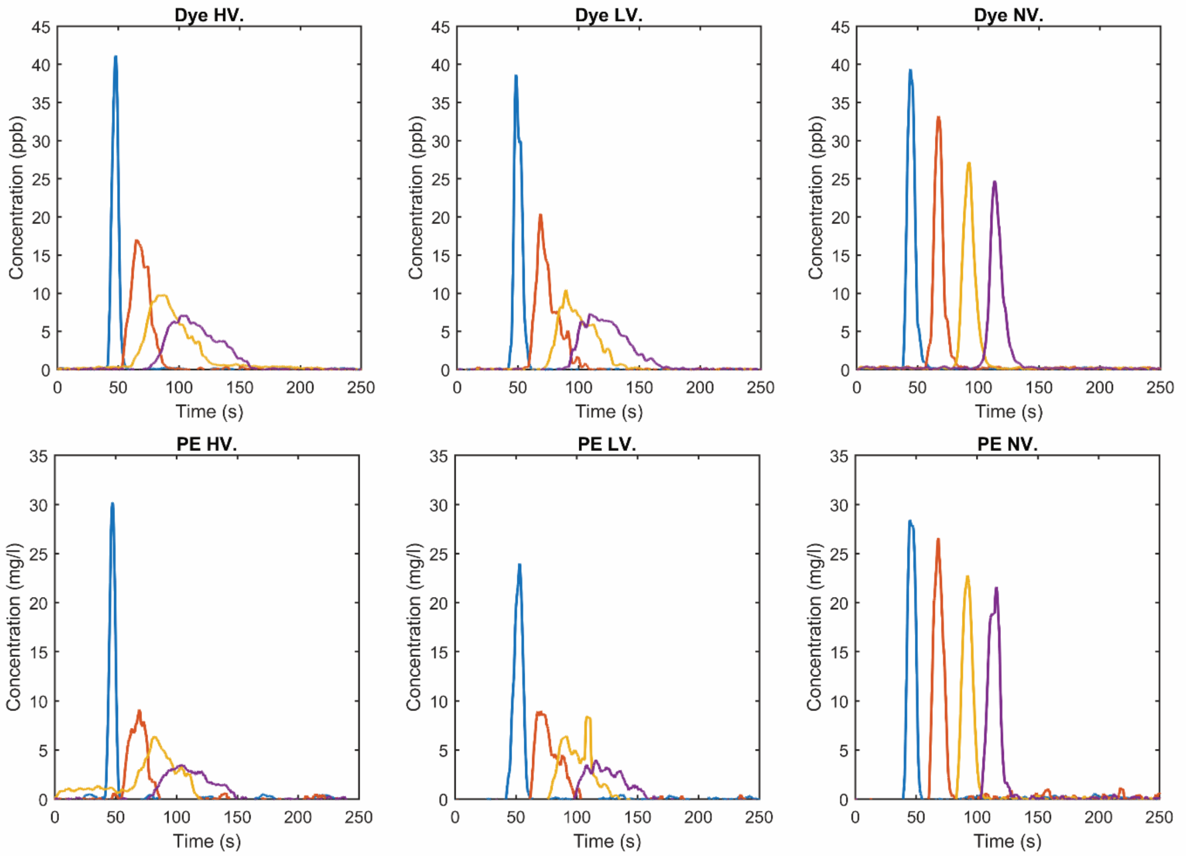

Fig. 4. *Response curves of instantaneous injections for dye (Rhodamine) and microplastic particles (PE) plotted as concentration (ppb for dye and mg/l for PE) against time (s) within HV, LV, and NV flow regimes at a depth-averaged velocity of 0.1059 m/s*

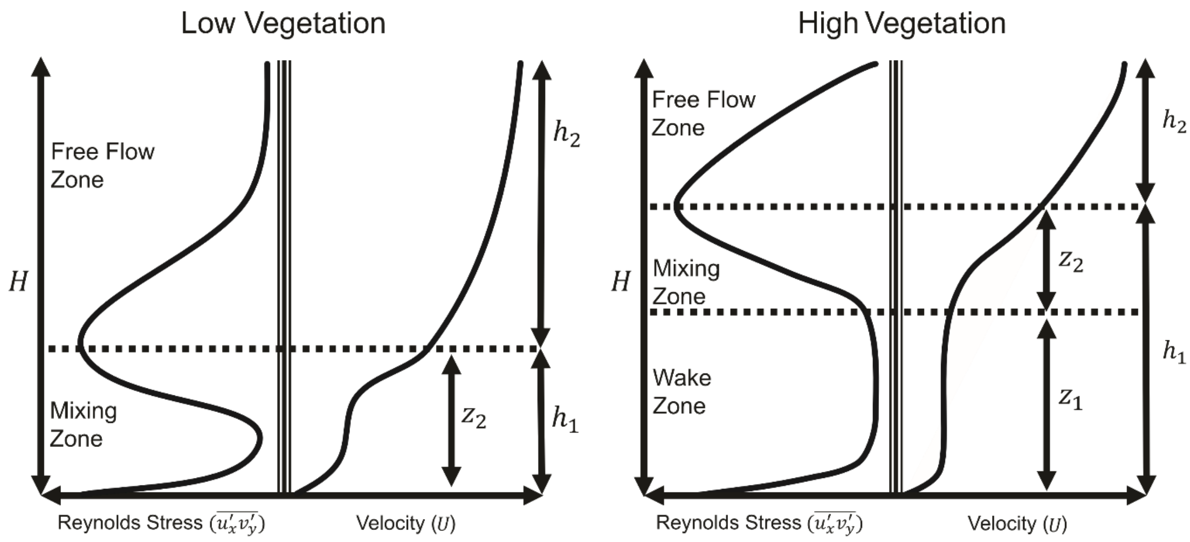

Fig. 5. *Conceptual model illustrating the relationship over a vertical profile between primary velocity and Reynolds stress through low and high submerged vegetation*

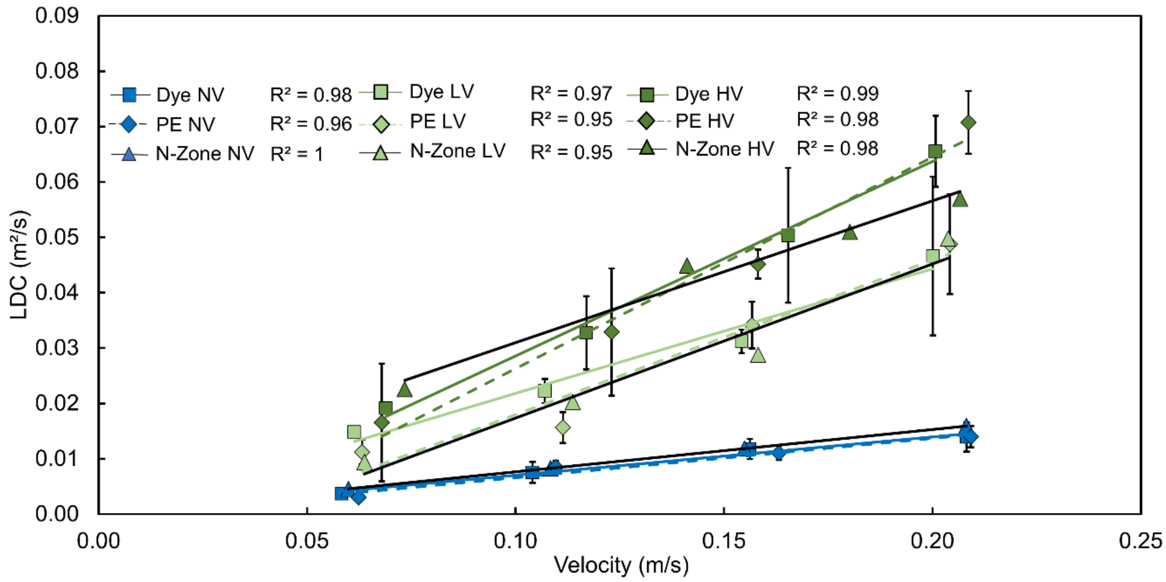

Fig. 6. *Mean LDC correlations for dye, PE, and theoretical N-zone values (± 95 % confidence intervals) versus velocity for the different vegetated conditons (NV, LV, HV)*

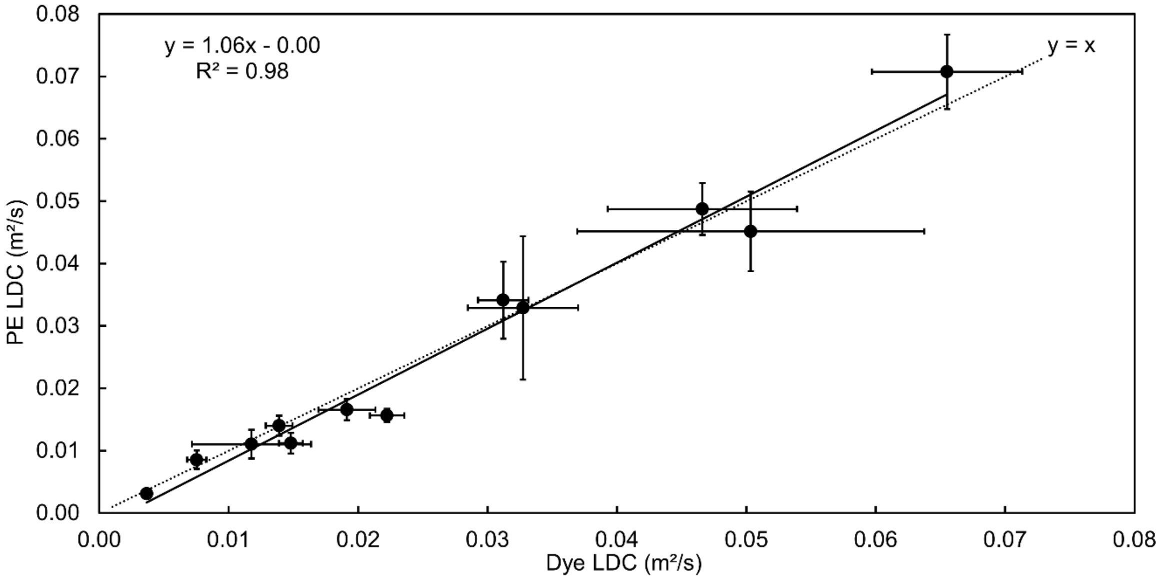

Fig. 7. *Mean PE LDC's versus mean dye LDC's for all conditions (± 95 % confidence intervals)*

Supplementary Materials

***Table S1**. LDC comparisons between dye, PE, and the N-Zone model with 95 % confidence intervals (±) and % difference for each experimental condition*

Vegetation Height (m)	Average Velocity (m/s)	Discharge (m^3/s)	Measured Dye	Measured PE	N-zone	% Difference Dye vs PE	% Difference Dye vs N-Zone	% Difference PE vs N-Zone
0	0.060	0.0051	0.0037 ± 0.0002	0.0031 ± 0.0006	0.0024	19.35	19.22	32.32
0	0.108	0.0092	0.0075 ± 0.0007	0.0085 ± 0.0015	0.0044	11.76	9.51	2.56
0	0.155	0.0132	0.0118 ± 0.0046	0.0110 ± 0.0023	0.0063	6.88	0.43	6.84
0	0.208	0.0177	0.0139 ± 0.0010	0.0140 ± 0.0016	0.0085	0.71	12.71	12.08
0.1	0.047	0.0040	0.0148 ± 0.0009	0.0112 ± 0.0039	0.0094	32.14	57.18	18.95
0.1	0.083	0.0071	0.0222 ± 0.0013	0.0156 ± 0.0034	0.0202	42.31	9.70	22.91
0.1	0.120	0.0102	0.0312 ± 0.0019	0.0341 ± 0.0062	0.0288	8.50	8.35	18.42
0.1	0.154	0.0131	0.0466 ± 0.0073	0.0487 ± 0.0042	0.0498	4.31	6.39	2.18
0.2	0.053	0.0045	0.0191 ± 0.0022	0.0166 ± 0.0017	0.0226	15.06	15.41	26.49
0.2	0.102	0.0087	0.0327 ± 0.0043	0.0329 ± 0.0115	0.0449	0.61	27.17	26.72
0.2	0.136	0.0116	0.0503 ± 0.0130	0.0451 ± 0.0064	0.0510	11.53	1.39	11.58
0.2	0.159	0.0135	0.0655 ± 0.0058	0.0707 ± 0.0060	0.0570	7.36	14.98	24.11